

# Spectroscopic and Laser Characteristics of Neodymium-doped Calcium Fluorophosphate

R. C. Ohlmann, K. B. Steinbruegge, and R. Mazelsky

Laser oscillations have been produced in large crystals of Nd<sup>3+</sup>-doped Ca<sub>5</sub>(PO<sub>4</sub>)<sub>3</sub>F (the mineral fluorapatite, whence the coined name FAP) at room temperature under both tungsten lamp and flash lamp excitation. The laser tests show that FAP:Nd crystals have four times greater gain per incident pump energy and over one and a half times greater differential (slope) energy efficiency than equal size YAG:Nd crystals. The fluorescence, excitation, and absorption spectra of FAP:Nd are partially polarized, as expected for Nd<sup>3+</sup> substituting Ca II sites of C<sub>1h</sub> symmetry. The fluorescence lifetime is 0.24 msec at 300°K. Laser oscillations occur at 1.0629 μ in π polarization ( $E||c$ ), which has 2.6 times the gain of σ polarization ( $E \perp c$ ).

## Introduction

Laser oscillations have been observed from a large number of crystals doped with neodymium ions.<sup>1,2</sup> However, only crystals that have some technological application have been studied extensively, e.g., yttrium aluminum garnet (YAG),<sup>3</sup> calcium tungstate,<sup>4</sup> and recently yttrium vanadate.<sup>5</sup> Crystals of YAG:Nd, since they provide a good combination of laser properties (low threshold and high efficiency) and optical, thermal, and mechanical properties, have been extensively used in our work as a standard with which to compare other Nd<sup>3+</sup>-doped crystals.

This paper presents the optical spectra and laser performance of a new neodymium-doped crystal, calcium fluorophosphate [Ca<sub>5</sub>(PO<sub>4</sub>)<sub>3</sub>F] (Ref. 6). The host crystal has the mineral name fluorapatite, from which we coined the name FAP. This material is distinguished by its high gain per incident power, its high output efficiency as shown in pulse laser tests, and by the fact that crystals of large size can be grown.

In principal, the laser characteristics, such as threshold power, gain, and efficiency, of a material can be theoretically predicted from its fluorescence and absorption properties. However, in actual practice, two major difficulties occur which make such a calculation unattractive. The absorption spectrum of Nd<sup>3+</sup>, especially in an anisotropic material, is complex, which makes it difficult to calculate the total absorption of radiative power from a pumping source. Furthermore,

the unpredictable internal losses of the laser material may be significant in determining its laser characteristics.

In order to overcome these difficulties partially, we have tried to evaluate the laser performance of FAP:Nd by comparing its properties with those of YAG:Nd. This was done by measuring and comparing the spectroscopic properties of these two materials, predicting their relative gain per unit population inversion, and then comparing their laser performance under as nearly identical conditions as possible.

In succeeding sections we report on the crystal growth of FAP, some of its crystallographic and physical properties, the spectroscopic properties of Nd<sup>3+</sup>-doped FAP, the results of pulse laser tests at room temperature, including threshold, efficiency, and scattering data, and observations of continuous laser oscillations at room temperature.

## Crystal Growth

Neodymium-doped fluorapatite is at best a quaternary system consisting of neodymium, calcium, phosphate, and fluoride ions, yielding the general composition Ca<sub>5-3x/2</sub>Nd<sub>x</sub>(PO<sub>4</sub>)<sub>3</sub>F. Johnson<sup>7</sup> has been successful in pulling large crystals of fluorapatite, pure and manganese doped, from the melt using the Czochralski method. Following a similar procedure, details of which are reported elsewhere,<sup>8</sup> we have pulled large (up to 25-cm long) crystals of FAP:Nd of high optical quality. The compound is congruently melting although the width of the phase field is relatively small. The melt is contained in iridium crucibles heated by 10-kHz power. An argon atmosphere protects the crucibles from oxidation. The temperature at the surface of the melt during growth is held at 1705°C as determined by optical pyrometer readings uncor-

All authors were with the Westinghouse Research Laboratories, Pittsburgh, Pennsylvania 15235; R. C. Ohlmann is now with Lockheed Research Laboratories, Palo Alto, California 94303.

Received 8 January 1968.

**Table I. Properties of Calcium Fluorophosphate**

Composition	$\text{Ca}_5(\text{PO}_4)_3\text{F}$
Density <sup>a</sup>	3.20 g/cm <sup>3</sup>
Melting point	1705 ± 10°C
Hardness <sup>b</sup>	377 Knoop (5-5.5 Moh)
Refractive index <sup>c</sup> (Na D line)	1.634 ( <i>o</i> ), 1.631 ( <i>e</i> )
Thermal expansivity <sup>d</sup> (300°C)	9 × 10 <sup>-6</sup> /°C
Thermal conductivity <sup>e</sup> (300°C)	0.020 W/cm <sup>-1</sup> °C (along <i>c</i> ) 0.024 W/cm <sup>-1</sup> °C (⊥ <i>c</i> )

<sup>a</sup> From x-ray data. There are  $1.91 \times 10^{22}$  Ca ions per cm<sup>3</sup>.

<sup>b</sup> J. A. Nelson (unpublished).

<sup>c</sup> Ordinary ray (*o*) refers to  $E \perp c$  axis polarization; extraordinary ray refers to  $E \parallel c$  axis polarization.

<sup>d</sup> C. Hager and J. Valentich Westinghouse Research Laboratories (unpublished). Hysteresis in the measurement prevented the detection of any anisotropy less than 5%.

<sup>e</sup> D. H. Damon, R. Mazelsky, W. Kramer, and P. A. Piotrowski (unpublished), measured on FAP:Nd (2 at.%) crystals.

rected for emissivity. Pull rates of 3-8 mm/h are used, and the seed crystal is rotated between 30-100 rpm.

Since Nd<sup>3+</sup> substitutes for Ca<sup>2+</sup> in the crystal, some type of charge compensation is required. Although we have used alkali metal ions as charge compensators, most crystals have been grown without purposely introducing a charge compensating ion. Charge neutrality in that case is maintained during crystal growth by a self-compensating mechanism such as the creation of calcium vacancies or the substitution of oxygen ions for fluorine ions. No differences were observed in the fluorescence spectra or in the laser properties whether or not the crystals were ion compensated or allowed to self-compensate. Analysis of the self-compensated crystals showed that they contained a neodymium concentration that was 52% of that of the melt.

### Crystallographic and Material Properties

The structure of apatite has been known for many years.<sup>9</sup> It has a hexagonal space group  $P6_3/m$  ( $C_{6h}^2$ ) and has two molecules of  $\text{Ca}_5(\text{PO}_4)_3\text{F}$  per unit cell. The F<sup>-</sup> ions lie in columns parallel to the *c* axis. Each F<sup>-</sup> ion is in the center of an equilateral triangle of Ca<sup>2+</sup> ions, the plane of the triangle being a mirror plane perpendicular to the *c* axis. Sixty percent of the Ca<sup>2+</sup> ions are in these sites, called Ca II sites, adjacent to F<sup>-</sup>. The Ca II sites have  $C_{1h}$  point symmetry and have nine near oxygen neighbors\* in addition to fluorine. The remaining 40% of the Ca<sup>2+</sup> ions are at Ca I sites having  $C_3$  point symmetry. These Ca I sites have six near oxygen neighbors with three other oxygen ions slightly further away.† Trivalent neodymium probably substitutes at a calcium site; polarization

\* The fluorine ion and four of the oxygen ions are about 2.3 Å from the Ca II site, another oxygen is 2.7 Å away, and four more oxygen ions are about 3.1 Å away.

† Six oxygen ions are about 2.3 Å from the Ca I site and three oxygen are 2.7 Å away.

data reported below are consistent with Ca II site substitution.

Some of the material properties of Nd<sup>3+</sup>-doped calcium fluorophosphate are listed in Table I. The thermal conductivity of YAG:Nd is three times greater than FAP:Nd so that heat may be more easily removed from YAG:Nd than from FAP:Nd lasers. However, the heat input per unit volume for a given average output power in a laser configuration may be made small for FAP:Nd lasers by using long rods. The low anisotropy of both the index of refraction and the thermal expansivity of FAP is important since the optical distortion of the material due to thermal effects is related to these parameters.

### Spectroscopic Properties

The fluorescence spectra from  $\text{Ca}_5(\text{PO}_4)_3\text{F}:\text{Nd}$  at 300°K are shown in Fig. 1. For clarity, the  $\sigma$  spectrum ( $E \perp c$ ) is drawn 2.5 times more intense relative to the  $\pi$  spectrum ( $E \parallel c$ ) than is observed. The intensity of the principal emission line at 1.0629  $\mu$  is 2.6 times stronger in  $\pi$  polarization than in  $\sigma$  polarization. It is about 6 Å wide. The fluorescence of FAP:Nd is somewhat unique compared with the fluorescence of Nd<sup>3+</sup> in many other host crystals in that a larger fraction of the emitted quanta is found in a single line. This statement is made quantitative in the next section in one particular case by comparing the fluorescence of Nd<sup>3+</sup> in YAG and in FAP.

The excitation spectrum of the 1.0629- $\mu$  fluorescence line from Nd<sup>3+</sup> in FAP is illustrated in Fig. 2. The influence of the spectral variation of the exciting photon flux has been removed from the shape of this curve, so the amplitude shown in Fig. 2 is proportional to the absorption of the crystal and its spectral quantum efficiency. The measured absorption spectrum of the

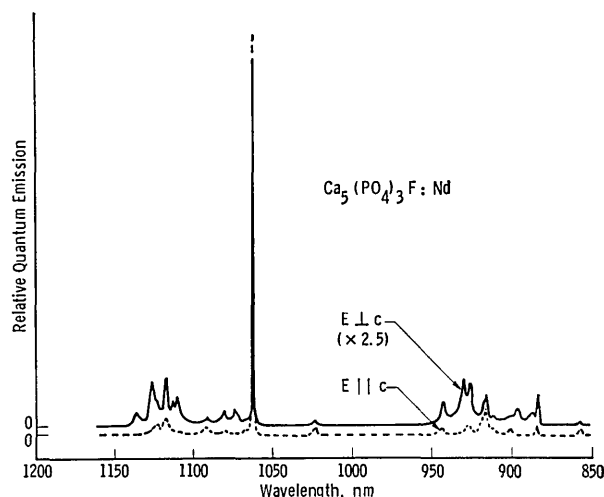


Fig. 1. Fluorescence spectra from  $\text{Ca}_5(\text{PO}_4)_3\text{F}:\text{Nd}$  at 300°K. The amplitude has been corrected for the spectral quantum sensitivity of the spectrometer and detector system. The amplifier gain for the  $E \perp c$  spectrum was 2.5 times greater than for the  $E \parallel c$  spectrum for clarity of presentation.

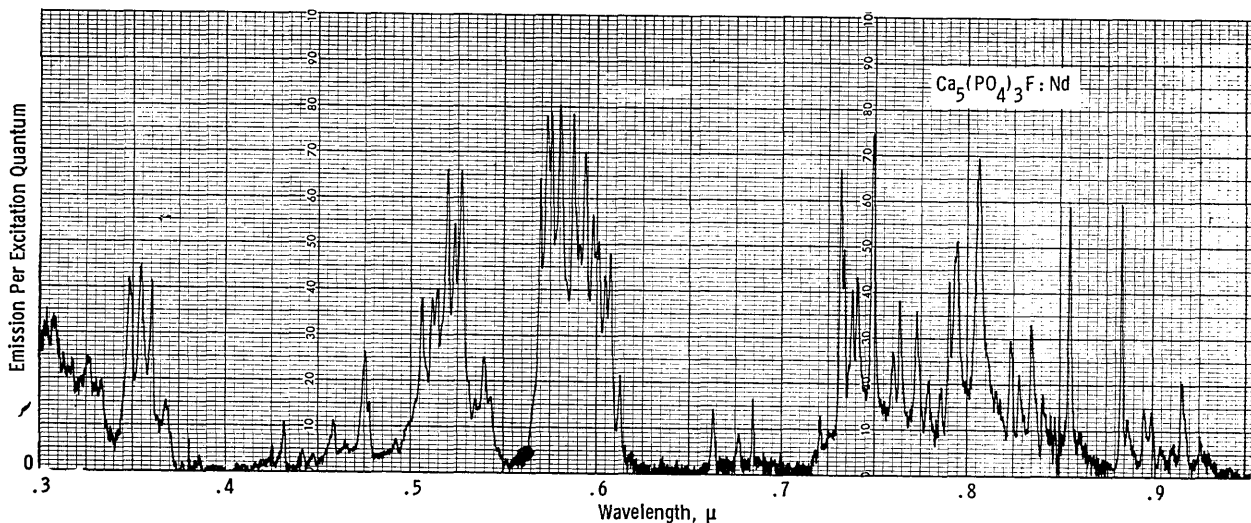


Fig. 2. The excitation spectrum of the 1.0629- $\mu$  fluorescence line from  $\text{Ca}_5(\text{PO}_4)_3\text{F:Nd}$  at 300°K. The amplitude has been corrected for the spectral variation of incident photon flux.

crystal has the same shape as the excitation spectrum, which implies that the quantum efficiency is independent of the exciting wavelength.

The energy levels of  $\text{Nd}^{3+}$  in  $\text{Ca}_5(\text{PO}_4)_3\text{F}$  have been determined by low temperature fluorescence and absorption studies. The spectrum of  $\text{Nd}^{3+}$  is particularly rich in lines, and only those details of the spectra pertinent to the laser performance are reported in this paper. The relative peak intensities, polarizations, and line widths of the fluorescence lines from FAP:Nd at 77°K are tabulated in Table II.

An attempt was made to distinguish lines due to purely electronic transitions from the vibronic lines and from those satellite lines due to  $\text{Nd}^{3+}$  not at its most common substitutional site. There are various techniques which may be used to discover which lines are vibronic,<sup>10</sup> such as the mirror symmetry about the electronic lines if the vibrational modes interact with the upper and lower states of the transition in the same manner. However, it was not possible to classify unambiguously all the lines by this technique owing to the complex spectra arising from the overlap of the electronic and vibronic lines. Therefore, we have simply selected the strongest and narrowest lines as electronic transitions (considering spectra obtained at 2°K and 4°K as well as 77°K), marking borderline cases as uncertain.

The crystal symmetry at either calcium site allows the degeneracy of the free ion states to be split into a set of Kramer doublets. Therefore, the ground state,  $^4I_{3/2}$ , splits into five levels, the next excited state,  $^4I_{11/2}$ , splits into six levels, and the  $^4F_{3/2}$  state splits into two levels. Figure 3 illustrates part of energy level structure determined by both fluorescence and absorption spectra. The levels indicated by dashes have not been clearly identified as purely electronic levels; they may involve vibrational energy. The transition that has participated in stimulated emission is illustrated in Fig. 3 by the large arrow.

The relative intensities of the spectral lines are the same in both the axial and  $\sigma$  spectra, which means that the transitions have electric dipole character. None of the lines listed in Table II are 100% polarized, although three electronic transitions have a ratio of six or more between the intensities of the two polarizations. There is a small possibility that scattering by crystal imperfections has caused some depolarization of the

Table II. Fluorescence Lines from FAP:Nd (0.4%) at 77°K

Wave-length $\lambda_{\text{air}} \text{ \AA}$	Frequency $\bar{\nu}_{\text{vac}} \text{ cm}^{-1}$	Peak intensity $I_{\pi}$	Peak intensity $I_{\sigma}$	Line width <sup>a</sup> $\Delta\bar{\nu} \text{ cm}^{-1}$	Energy difference <sup>b</sup> (11310- $\bar{\nu}$ ) $\text{cm}^{-1}$
8825	11328	2	5	11	-18 <sup>s</sup>
8839	11310	19	40	5 <sup>c</sup>	0 <sup>e</sup>
9150	10926	12	5	9	384 <sup>s</sup>
9163	10910	120	63	8	400 <sup>e</sup>
9185	10884	18	14	8	426 <sup>ev</sup>
9258	10798	34	81	13	512 <sup>e</sup>
9290	10761	3	11	20	549 <sup>v</sup>
9308	10741	9	72	15	569 <sup>s</sup>
9429	10603	20	32	15	707 <sup>ev</sup>
10613	9420	27	12	7	1890 <sup>s</sup>
10629	9406	558 <sup>e</sup>	264 <sup>e</sup>	4 <sup>c</sup>	1904 <sup>e</sup>
11102	9005	4	32	11	2305 <sup>e</sup>
11133	8980	2	7	14	2330 <sup>v</sup>
11175	8946	18	35	18	2364 <sup>e</sup>
11225	8906	16	13	18	2404 <sup>e</sup>
11259	8879	6	38	14	2431 <sup>e</sup>
11362	8799	3	15	18	2511 <sup>e</sup>
13348	7490	—	25	20	3810 <sup>e</sup>

<sup>a</sup>  $\Delta\bar{\nu} = (2/\pi)$  area/peak intensity, applicable to a Lorentzian line shape, was used to obtain the line width. The resolution was about 4  $\text{cm}^{-1}$ .

<sup>b</sup> s: satellite line not seen in all samples; e: probably electronic transition; ev: either electronic or vibronic; v: probably vibronic in origin.

<sup>c</sup> Resolution limited.

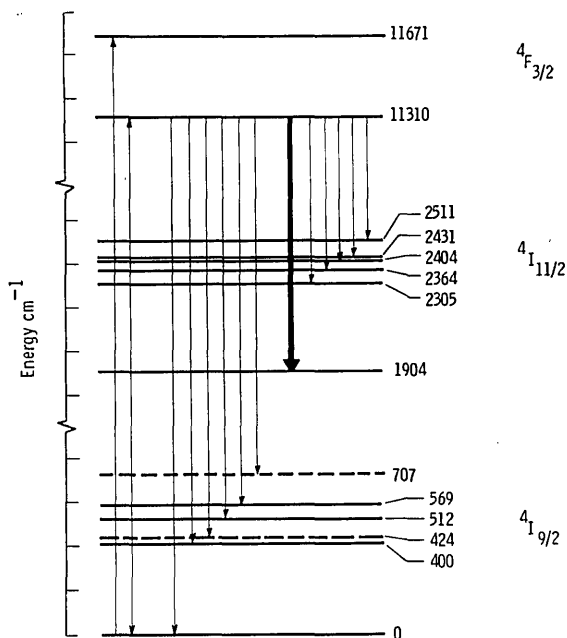


Fig. 3. Energy levels of three terms of  $\text{Nd}^{3+}$  in  $\text{Ca}_5(\text{PO}_4)_3\text{F}$ . The dashed lines represent levels which may contain vibrational energy. Fluorescence due to transitions from both  ${}^4F_{3/2}$  states to all the lower states is observed at  $300^\circ\text{K}$ . The transitions shown by arrows are observed at  $77^\circ\text{K}$ . The laser transition is indicated by a heavy arrow.

observed fluorescence, although tests indicate that a depolarization by more than a few percent due to scattering should not occur with the crystals used. The fact that 100% polarized lines are not observed either in fluorescence or absorption is consistent with the hypothesis that  $\text{Nd}^{3+}$  substitutes at Ca II sites  $C_{1h}$  symmetry by the following reasoning.

All of the spin doublets in  $\text{Nd}^{3+}$  transform<sup>11</sup> as the  $\Gamma_3$  and  $\Gamma_4$  complex conjugate representations of the  $C_{1h}$  group. Since  $\Gamma_3$  and  $\Gamma_4$  states are degenerate, dipole matrix elements between any two pair of ( $\Gamma_3$ ,  $\Gamma_4$ ) states are nonzero for both polarizations, which means that partially polarized spectra should be observed if  $\text{Nd}^{3+}$  ions are in  $C_{1h}$  symmetry. On the other hand, if  $\text{Nd}^{3+}$  substitutes at Ca I sites having  $C_3$  symmetry, the spin doublets transform either as the complex conjugate representations  $\Gamma_4$  and  $\Gamma_5$  or as the  $\Gamma_6$  representation. Transitions between  $\Gamma_6$ - $\Gamma_6$  are  $\pi$  polarized, those between  $\Gamma_6$ -( $\Gamma_4$ ,  $\Gamma_5$ ) pairs are  $\pi$  polarized, and those between ( $\Gamma_4$ ,  $\Gamma_5$ )-( $\Gamma_4$ ,  $\Gamma_5$ ) pairs are partially polarized. Therefore, many of the spectral lines would be 100% polarized if  $\text{Nd}^{3+}$  ions are in  $C_3$  symmetry, which is contrary to our data.

It is possible that the symmetry of a Ca I site is disturbed when  $\text{Nd}^{3+}$  is at that site due to a nearby charge compensating ion. However, a comparison of the spectra from several crystals of FAP:Nd, both with and without charge compensating ions such as sodium and potassium added to the melt, revealed only very small changes in the spectra. Some of the samples have about 1% of their emission appearing as

very weak lines which might be attributed to  $\text{Nd}^{3+}$  in sites which differed from those containing most of the  $\text{Nd}^{3+}$  ions. The conclusion that  $\text{Nd}^{3+}$  primarily substitutes at the Ca II sites is in agreement with the spin resonance spectra of  $\text{Nd}^{3+}$  in FAP recently measured by Wagner.<sup>12</sup>

### Spectral Quantum Efficiency

Although the shape of the fluorescence spectrum of FAP:Nd suggests that the stimulated emission cross section is high at  $1.0629 \mu$ , particularly for  $\pi$  polarization, the fluorescence quantum efficiency is required to determine the importance of nonradiative decay processes. The spectral quantum efficiency of a crystal of FAP:Nd (0.4 at. %) was obtained relative to a crystal of YAG:Nd (1.3 at. %), each crystal being in the form of a 6-mm  $\times$  3-mm  $\times$  3-mm slab. More specifically, we determined the relative fluorescence rate at the peak of strongest emission line in each material ( $1.0629 \mu$  for FAP:Nd and  $1.0642 \mu$  for YAG:Nd)\* for the same rate of absorption of exciting photons by each material. This quantity multiplied by the inverse square of the index of refraction ratio is equal to relative stimulated emission gain of the two materials (near threshold) for the same power absorbed.

Two independent measurement techniques were used to compare the two crystals. In the simplest method, each crystal was excited in turn by  $5222\text{-}\text{\AA}$  radiation ( $100\text{-}\text{\AA}$  bandwidth) and the fluorescence intensity at the peak of the main line of each was measured using about  $1\text{-}\text{\AA}$  resolution on the spectrometer. Emission from the FAP:Nd crystal was observed along the  $c$  axis so that only  $\sigma$  polarization was detected. The intensity from YAG:Nd was multiplied by 1.28, the square of the index of refraction ratio, i.e.  $(1.82/1.63)^2$ , to account for the smaller internal solid angle used to collect the fluorescence from YAG:Nd. The transmission of the exciting light as determined by a sample in, sample out method, was 69% for each sample. After correcting for Fresnel surface reflection, the absorption ratio was known. Dividing the fluorescence intensity ratio by the relative absorption gave the result that the  $\sigma$  polarized emission from FAP:Nd is 0.85 as intense as the emission from YAG:Nd for the same absorption. Since  $\pi$  polarized fluorescence from FAP:Nd is 2.6 times more intense than the  $\sigma$  fluorescence, the  $\pi$  polarized fluorescence from FAP:Nd is 2.3 times greater than from YAG:Nd at the peak of the main emission line of each for the same absorption.

The second method required a careful measurement of the shape of the total fluorescence spectra at room temperature from the two crystals. The analysis of the spectra revealed that 33% of the  $\pi$  polarized fluorescence from FAP:Nd is emitted in the principal line compared with 18% in the main line from YAG:Nd. Using a carefully controlled geometry, the

\* Reference 3 reports laser emission from YAG:Nd at  $1.0648 \mu$ . However, we measure  $1.06415 \mu$  on two independently calibrated spectrometers.

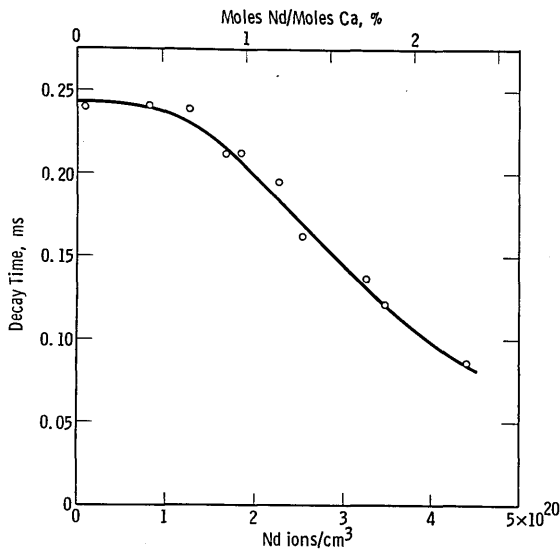


Fig. 4. Observed decay time of the Nd<sup>3+</sup> fluorescence from FAP:Nd at 300°K as a function of the concentration of Nd ions in the crystal as determined by x-ray fluorescence analysis.

relative intensities from the two crystals were measured using an interference filter to collect the fluorescence. Since this filter passed several lines, appropriate calculations were required to obtain the relative peak intensity. The result was that FAP:Nd (0.4%) has a peak intensity for  $\pi$  polarization that is 2.9 times that from YAG:Nd (1.3%) for the same absorbed power.

Averaging the results of the two methods gave 2.65 times higher peak intensity in  $\pi$  polarization from FAP:Nd than from YAG:Nd. However, our decay time measurements indicate that the YAG:Nd (1.3%) crystal has only about 80% of the quantum efficiency of YAG having 0.7% Nd. Therefore, at low concentrations, the fluorescence intensity of FAP:Nd ( $\pi$ ) is  $2.1 \pm 0.3$  times that of YAG:Nd for the same absorbed power, and thus the gain for  $\pi$  polarized radiation in FAP:Nd is  $2.7 \pm 0.3$  times that in YAG: per unit absorbed power.

The laser transition cross section at the peak of the line was determined by measuring the absorption of  $\pi$  polarized light by a 5-cm long rod at 297°K. An absorption coefficient of  $0.008 \text{ cm}^{-1}$  was found at  $1.0629 \mu$  for a rod containing  $2.1 \times 10^{20}$  Nd ions/cm<sup>3</sup>. The population density of the level  $1904 \text{ cm}^{-1}$  above the ground state at  $kT = 207 \text{ cm}^{-1}$  is  $N_0[\exp(-1904/207)]/Z$ , where  $Z$  is the partition function  $\sum_0^n \exp[-E_i/kT]$ . At 297°K we find  $Z = 1.33$  using the level scheme in Fig. 3. The population density of the  $1904 \text{ cm}^{-1}$  level is then  $0.75 \times 10^{-4}$  of the total population at 297°K, i.e.,  $1.6 \times 10^{16}$  ions/cm<sup>3</sup>. Therefore, the peak absorption cross section  $\sigma_{L\pi}$  of the laser transition is  $(5 \pm 1) \times 10^{-19} \text{ cm}^2$ . This number is of limited use in calculating the pumping power required to reach threshold since the constant of proportionality between the electrical power to a lamp and the population inversion is very difficult to calculate for the complex absorption spectrum of FAP:Nd.

We also may calculate the radiative transition rate  $\tau^{-1}$  from the absorption cross section by the relation<sup>13</sup>:

$$\tau^{-1} = 8\pi n^2 \bar{\nu}^{-2} c \int (\frac{2}{3}\sigma_{\sigma} + \frac{1}{3}\sigma_{\pi}) d\bar{\nu}, \quad (1)$$

where  $n$  is the index of refraction,  $\bar{\nu}$  is the frequency in  $\text{cm}^{-1}$ , and we assume the degeneracy of the upper and lower state is the same. This relationship should hold for the radiative transition rate of the laser transition, but a comparison of that rate with the measured decay rate requires a detailed knowledge of the fluorescence spectra. The total radiative transition rate is the sum of rates of all the transitions from the emitting states. In addition, the relative intensities of each of the fluorescence lines are proportional to their relative transition rates. We determined from the room temperature fluorescence spectra that the number of photons of both polarizations emitted at  $1.0629 \mu$  is 0.17 of the total number of emitted photons. Substituting  $\int \sigma_{L\pi} d\bar{\nu} = 41 \times 10^{-19} \text{ cm}$  and  $\int \sigma_{L\sigma} \bar{\nu} = (41/2.6) \times 10^{-19} \text{ cm}$  into Eq. (1) gives a decay time for the laser transition of 2.33 msec. Therefore, the total radiative decay time should be  $2.33 \times 0.17/0.85 = 0.47$  msec. The extra factor of 0.85 arises since the lower  ${}^4F_{3/2}$  level has 85% of the total population of both the  ${}^4F_{3/2}$  levels at room temperature. At room temperature and for low concentrations of Nd in FAP the measured decay time is 0.24 msec, as illustrated in Fig. 4. The decay time calculated above is about twice as long as measured, which may be attributed to the neglect of non-radiative and longer wavelength radiative transitions in the calculations.

The spectroscopic study of YAG:Nd shows that 0.18 of the emitted photons are in the  $1.0642 \mu$  fluorescence line. That line originates from the upper  ${}^4F_{3/2}$  level which has only 40% of the total population of both  ${}^4F_{3/2}$  levels at room temperature. At low Nd concentrations, the measured decay time is 0.27 msec, decreasing to 0.23 msec at 1.3 at. % Nd. If we assume that the radiative decay time of the laser transition is  $0.27 \times 0.4/0.18 = 0.59$  msec, then by substituting into Eq. (1) we calculate that  $\int \sigma_L(\text{YAG}) d\bar{\nu} = 80 \times 10^{-19} \text{ cm}$ . With the measured line width of  $6.5 \text{ \AA}$ , the peak value is  $\sigma_L(\text{YAG}) = 8 \times 10^{-19} \text{ cm}^2$ . The same factor of two errors may be present in the radiative decay time as occurred in the calculation on FAP:Nd, so that a closer estimate may be  $\sigma_L(\text{YAG}) = 4 \times 10^{-19} \text{ cm}^2$ .\*

### Pulse Laser Characteristics

A large number of laser rods of FAP:Nd have been fabricated and their laser performance measured. These have varied in size from 3 mm to 9 mm in diameter and 20 mm to 250 mm in length. The results of these measurements may be most meaningfully summarized by reporting a direct comparison between the laser performance of YAG:Nd and FAP:Nd. This comparison was performed on identical size rods (6.4-mm diam and 38-mm long) using external resona-

\* A value of  $\sigma_L(\text{YAG}) = 2.7 \times 10^{-19} \text{ cm}^2$  is reported by J. K. Neeland and V. Evtuhov, Phys. Rev. **156**, 244 (1967).

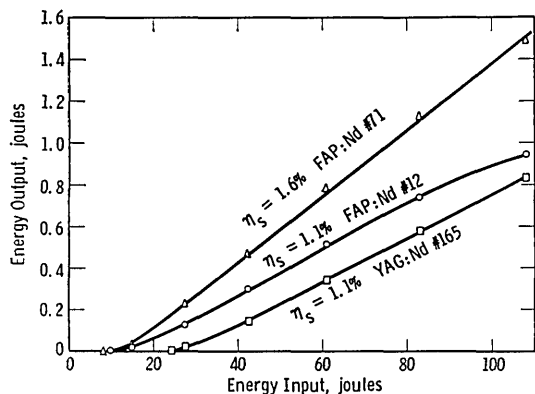


Fig. 5. Laser output vs input energy into a flashlamp for laser rods 6.4-mm diam by 38-mm long in a cylindrical pump cavity. Plane cavity resonators of 99% and 35% reflectivities were used.

tor mirrors and the same pumping cavity. We believe that the differences observed are entirely due to the material properties of the rods studied and that the conditions of the tests do not affect the comparison.

The YAG:Nd rod used for comparison was commercially purchased\* in 1966. It had a laser threshold and efficiency under pulse excitation which equaled or exceeded several other YAG:Nd rods which were tested. Therefore, we believe the rod is of a quality at least typical of many YAG:Nd laser rods. However, YAG:Nd rods having much lower scattering loss than our material have been reported.<sup>14</sup> The effect of scattering on our comparison is discussed.

In making the comparison tests the laser rods, having flat and parallel ends, were placed in a 28-cm resonator cavity which had external plane dielectric-coated mirrors. One mirror was 99% reflecting; the output mirror was selected from one of several mirrors having reflectivities from 35% to 99%. The laser rods were excited by a PEK Xe 1-3 flashlamp (5-mm diam and 75-mm long arc) having a flash duration of 800  $\mu$ sec. The pumping enclosure was a 70-mm i.d., aluminized glass cylinder 75 mm long. The laser rods were surrounded by a 1.5-mm thick, 50% aqueous solution of sodium nitrite which filtered out the uv and completely prevented the rods from coloring.<sup>15</sup> Output power was observed with a phototube, and output energy was measured with a TRG model 100 thermopile. We have found that the results obtained with this apparatus are reproducible to 5%.

The threshold pump energy for laser action and the output energy for a range of pump energies were measured for each of four FAP:Nd rods and the YAG:Nd rod using eight different values of the output resonator reflectivity. Each of the rods had a maximum slope efficiency (differential output energy/input energy) when tested using the 35% reflecting output mirror. Figure 5 illustrates the measured output energy from

the YAG:Nd rod and two of the FAP:Nd rods (using the 35% reflecting resonator) as a function of the energy input into the lamps. The data from the other two FAP:Nd rods lies between the plotted curves. In Fig. 5 the energy input was considered equal to the initial energy stored in the capacitor without correction for electrical losses or incomplete capacitor discharge.

It is clear from Fig. 5 that the FAP:Nd rods have lower thresholds and equal or higher efficiencies than the YAG:Nd rod. The variation among the FAP:Nd rods have some correlation with the optical quality. The qualitative observation of the large angle scattering of a He-Ne laser beam (6328  $\text{\AA}$ ) propagating down each rod showed that all FAP:Nd rods scattered more than the YAG:Nd rod. However, the more efficient FAP:Nd rods had smaller scattering than the less efficient FAP:Nd rods.

Quantitative comparisons of the losses and gain during laser operation were obtained by use of the well-known technique relating losses and laser thresholds.<sup>16</sup> To review, at threshold, the following relation holds<sup>1</sup>:

$$T^2 R_1 R_2 \exp[2(\alpha - \alpha_s)L] = 1, \quad (2)$$

where  $\alpha$  = gain coefficient;  $\alpha_s$  = distributed loss coefficient (including scattering and absorption at the laser wavelength);  $L$  = length of laser material;  $T$  = single pass transmission within the laser cavity excluding distributed losses; and  $R_1, R_2$  = resonator reflectivities.

For a four-level material, i.e., one with no population in the terminal state of the laser transition,

$$\alpha = \sigma N_i = C E_T, \quad (3)$$

where  $\sigma$  = transition cross section of the laser transition;  $N_i$  = population density of the initial state of the laser transition at threshold;  $E_T$  = threshold energy into excitation lamp corrected for spectral variations of the lamp with energy; and  $C$  = proportionality constant: gain per unit pump energy.

In real four-level laser material there is a small terminal state population so that, while the second half of Eq. (3) may be valid, the first half should be written:  $\alpha = \sigma(N_i - N_t)$ , where  $N_t$  is the terminal state population density weighted by the ratio of the degeneracies of the initial and final states. We continue to use Eq. (3) and include the effective absorption  $\sigma N_t$  in with the distributed loss coefficient.

The spectral distribution and pulse duration of the lamp is not constant at very low values of  $E_T$ , and this is one cause of nonlinearity between  $N_i$  and  $E_T$ . This effect has been corrected for by observing the integrated fluorescence signal from the crystals (without resonators or pumping reflectors to keep the stimulated emission negligible) as a function of  $E_T$  and then correcting the values of  $E_T$  to maintain linearity. This correction was significant, amounting to an effective  $E_T$  that was 3.2 J less than the energy stored in the capacitor for all values of stored energy above 8 J. Examples of lower values of the effective lamp energy are 0.8 J for 3-J stored energy and 2.2 J for 5-J stored energy.

\* Electronics (formerly Linde) Division of Union Carbide Corporation.

Table III. Results of Pulse Laser Tests

Material <sup>a,b</sup>	Loss coefficient $\alpha_s, \text{cm}^{-1}$	Gain/J $c, \text{cm}^{-1} \text{J}^{-1}$	Threshold <sup>c</sup> (95% refl.) J	Threshold <sup>c</sup> (35% refl.) J	Max. slope <sup>d</sup> eff., %
FAP:Nd #12	$\pm 10\%$	$\pm 5\%$	$\pm 0.2 \text{ J}$	$\pm 0.2 \text{ J}$	$\pm 0.05$
FAP:Nd #12	0.11	0.035	6.0	9.8	1.1
FAP:Nd #1	0.07	0.027	5.8	11.0	1.1
FAP:Nd #57A	0.07	0.027	5.8	11.2	1.2
FAP:Nd #71	0.05	0.035	4.4	8.6	1.6
YAG:Nd #165	0.01	0.0071	6.1	24.5	1.1

<sup>a</sup> All laser rods 6.4-mm diam  $\times$  38-mm long. FAP rods oriented with axis  $\perp c$  direction.

<sup>b</sup> Materials all have  $2.1 \times 10^{20}$  Nd ions/cm<sup>3</sup>; equivalent to 1.1 at. % Nd in FAP and 1.5 at. % Nd in YAG.

<sup>c</sup> Measured threshold, not corrected for spectrum change of the lamp.

<sup>d</sup> Using 35% reflectivity output mirror.

By substituting Eq. (3) into Eq. (2) and rearranging terms, we obtain:

$$CE_T = -(2L)^{-1} \ln R_1 R_2 + (\alpha_s - L^{-1} \ln T). \quad (4)$$

A linear relationship between  $E_T$  and  $-(2L)^{-1} \ln R_1 R_2$  should be observed with an intercept at  $E_T = 0$  of  $\alpha_{se} = \alpha_s - L^{-1} \ln T$ . The value of  $\alpha_{se}$  is an effective distributed loss coefficient indicative of crystal quality. Although we attempted to have  $T = 1$ , scattering at the crystal face or Fresnel reflection at the crystal-air boundary may have made  $T < 1$ . Furthermore, as Findlay and Clay<sup>16</sup> have pointed out, the external reflectors and the plane ends of the rod may form a Fabry-Perot system with a higher effective reflectivity than given by  $R_1 R_2$ . However, no change in  $\alpha_{se}$  was noted whether or not the rods were antireflection-coated so that our calculations of  $\alpha_s$  assume  $T = 1$  and use the actual values of  $R_1$  and  $R_2$ . Note that an  $\alpha_s$  value obtained from threshold measurements is for the best path or filament through the rod; the average quality of the rod may be considerably poorer.

The factor  $C$ , which has also been experimentally determined from the dependence of  $E_T$  on  $-(2L)^{-1} \ln R_1 R_2$ , is the gain coefficient per joule of pump energy. Although  $C$  will depend on the efficiency of the pumping cavity, the spectrum of the lamp, and the pulse duration, a comparison of its values between two materials reveals their relative efficiency of excitation of the best filament if the ratio of their cross sections  $\sigma$  are known and they have similar decay rates.

A least squares fit of the corrected threshold measurements at eight values of output reflectivity was made to Eq. (4) using linear regression theory. There is a good fit of the data to Eq. (4) since the standard deviation of the linear fit from the measured values is less than 0.3 J for all samples, which is of the order of the experimental precision. The 50% confidence interval of the fitted parameters (which follow a chi square distribution) are: for  $C$ , about 5% of its value; for  $\alpha_s$ , about 10% of its value for all sets of data. Table III lists the calculated values of  $\alpha$  and  $C$ , as well as the measured (uncorrected) threshold energies for 95% and 35% output reflectivity and the maximum slope efficiency obtained from each of the four FAP:Nd rods and one YAG:Nd rod.

In addition to the threshold and output energy measurements, the beam divergence of each of the FAP:Nd laser rods was determined. The definition of beam divergence is not obvious for a multimode, multilobe, laser beam. However, the photographs of the laser output from our rods showed spots that were roughly circular. Therefore, we define the beam divergence as the full angle in the far field which contains 50% of the output energy. The measurement was made using a long focal length lens, variable apertures, and the TRG thermopile. Typical values for the beam divergence from our FAP:Nd rods are between 3 mrad and 6 mrad.

### Discussion of Pulse Laser Tests

The loss coefficients reported in Table III are relatively large for good laser crystals. For example, some YAG:Nd rods have been reported<sup>14</sup> to have losses less than  $0.001 \text{ cm}^{-1}$ . The value of  $0.01 \text{ cm}^{-1}$  for our YAG:Nd rod may be an upper limit due to the measurement technique; the 28-cm spacing between plane resonators accentuates the effects of small angle scattering. Thus, even the best filament through the rod may show a larger scattering loss than would be measured using a smaller cavity with curved mirrors. The crystal quality of the FAP:Nd crystals tested is not as good as the quality of the YAG:Nd crystal. The loss coefficient of the FAP:Nd rods is several times the limit of  $0.008 \text{ cm}^{-1}$  expected from the absorption due to excitations from the terminal state at room temperature.

The value of  $C$ , the gain coefficient per input joule, is about four to five times larger for the FAP:Nd rods than for the YAG:Nd rod. Using the relationship between the excited state population at threshold and the pumping energy, as expressed by Eq. (3), we calculate that  $N_i \approx 6 \times 10^{16} E_T$  for FAP:Nd and  $N_i \approx 3.5 \times 10^{16} E_T$  for YAG:Nd in our apparatus. Since the decay times of the rods are almost equal, the greater excited state population achieved in FAP:Nd for the same excitation must be due to a greater absorption of the pump radiation by FAP:Nd than by YAG:Nd. This is confirmed by the higher slope efficiencies of the FAP:Nd laser rods.

The maximum slope efficiency and the value of  $C$  obtained from threshold measurements are related.

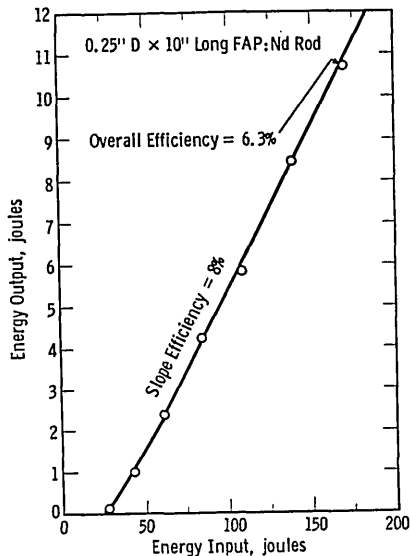


Fig. 6. Laser output vs input energy in a flashlamp for a FAP:Nd laser rod 6.3-mm diam by 250-mm long in a close-coupled pump enclosure. One external 99% reflecting mirror was used. The output was from the uncoated end of the rod.

Before coherent oscillations begin, the energy released by the crystal from the upper state is equal to:

$$E_f = \int \tau^{-1} h\nu V N(t) dt, \quad (5)$$

where  $V$  is the crystal volume. When pumping at the threshold energy we approximate  $\int N(t) dt$  by  $N_i T$  rather than solve the differential equation involving the decay time and time dependence of the lamp, e.g., for the 800- $\mu$ sec lamp pulse we estimate  $T = 400$   $\mu$ sec, when we use the threshold population density for  $N_i$ . Substituting for  $N_i$  from Eq. (3) and assuming 100% quantum efficiency, the fluorescence energy at threshold equals:

$$E_f \approx h\nu VTC(\sigma\tau)^{-1} E_T. \quad (6)$$

Above threshold, neglecting scattering, the excess pump energy appears as laser output for high output coupling. Therefore, the slope efficiency  $\eta_s$  should be expressed by:

$$\eta_s \leq h\nu_E VTC/\sigma\tau. \quad (7)$$

With  $C = 0.03 \text{ cm}^{-1} \text{ J}^{-1}$  for the FAP:Nd rods in our pumping cavity, we obtain  $\eta_s \approx 2\%$ , close to the measured values shown in Table III. Since only 0.75 of this is expected for  $\alpha = 0.05$ ,  $L = 3.8 \text{ cm}$ ,  $R_1 = 1$ , and  $R_2 = 0.35$  by the theory of Miles and Goldstein,<sup>17</sup> the agreement is even closer.

Many of the results of the pulse tests discussed above are dependent on the pumping configuration and the size of the laser rods. They are of general interest in that they demonstrate a consistency with the spectroscopic measurements and they also allow a comparison with a YAG:Nd laser rod. The scattering of the YAG:Nd rod appears small enough to have a negligible effect on its slope efficiency. On the other hand, the slope efficiencies of the FAP:Nd rods clearly are affected

by scattering of the stimulated emission since the higher efficiency rods have a smaller average scattering loss. Note that the average scattering loss through the rod is somewhat greater than the loss in the best filament as evidenced by the curvature of the output vs input curves (shown in Fig. 5) near threshold.

Higher efficiencies are usually obtained with larger sizes of laser rods since better coupling to the pump lamp is possible. As an example, a FAP:Nd rod 6.3-mm diam by 250-mm long was tested in a close coupled pumping cavity: a block of magnesium carbonate hollowed to contain a flashlamp and rod. With one 99% reflecting external mirror and the Fresnel surface reflection as the output reflector, a slope efficiency of 8%, and an over-all efficiency of 6.3% at 10.7-J output was reached. The laser output vs energy input for this rod is illustrated in Fig. 6.

### Continuous Laser Characteristics

Several FAP:Nd rods have been made to oscillate continuously at room temperature using tungsten lamp excitation. The data at this time are not as extensive as those from the pulse laser tests. The pumping cavity used for these experiments was designed more for repeatability of pumping than for efficiency of pumping. For example, in a highly efficient 15-cm spherical pumping cavity,<sup>18</sup> a particular 2 mm x 20 mm FAP:Nd rod has a threshold of 145 W when excited by a tungsten iodide lamp rated at 100 W. However, the same rod in a 10-cm diam by 5-cm long aluminumized cylindrical cavity has a 590-W threshold when excited by a tungsten iodide lamp rated at 500 W. These values were obtained using dielectric reflectors on the rod ends, one with a 50-mm radius of curvature and 99.9% reflecting and the other flat and 99.1% reflecting.

The cylindrical pumping cavity was used for comparative testing of various FAP:Nd and YAG:Nd rods. External dielectric reflectors of 99.9% and either 97% or 99% reflectivity were used for the resonator cavity.

Table IV. Results of Continuous Laser Tests

Material <sup>a</sup>	Output mirror <sup>b</sup> refl. (%)	Threshold <sup>c</sup> (W)	Output at 1-kW input (mW)	Max. slope eff. (%)
FAP:Nd #90A	99	535(665)	140	0.042
3-mm diam x 30 mm				
FAP:Nd #90B	99	520(695)	95	0.031
3-mm diam x 30 mm	97	590(735)	75	0.045
FAP:Nd #93	99	580(740)	80	0.031
3-mm diam x 36 mm	97	700(780)	131	0.060
YAG:Nd	99	600(660)	273	0.080
3-mm diam x 30 mm	97	780(795)	115	0.069

<sup>a</sup> All FAP rods oriented so the c axis is perpendicular to the rod axis.

<sup>b</sup> One resonator was 99.9% reflecting.

<sup>c</sup> Initial threshold is reported first; the threshold in parentheses is obtained by extrapolation of the linear part output vs input curves to zero output.

These mirrors have a 31.7-cm radius of curvature and were spaced 16 cm apart. Each laser rod had flat ends on which was evaporated an antireflection coating of  $\text{MgF}_2$ . The tungsten iodide pumping lamp has a 2-mm diam by 50-mm long filament rated at 500 W.

The results of the continuous tests are tabulated in Table IV. The observed threshold power into the lamp, the laser output power with 1 kW into the lamp, and the maximum slope efficiency of each rod are reported. The threshold powers of the FAP:Nd rods are about 80% of the threshold obtained by extrapolating the linear region of output vs input power to zero output. This indicates that the average losses are greater than those of the best filament.

The maximum slope efficiencies are more than an order of magnitude less than can be obtained in an efficient pumping system using longer rods and more nearly optimum output coupling. However, the significance of Table IV lies in the comparison between the various rods. The threshold powers of the various rods are not considerably different, yet the YAG:Nd rod has 1.3 times the efficiency of the highest efficiency FAP:Nd rod. This is not in accordance with the pulse laser tests. The explanation may be found by considering the output coupling in the presence of losses. The effective output coupling is<sup>17</sup>

$$[1 - (2\alpha_s L / \ln R)]^{-1}. \quad (8)$$

It is clear from Table III that the slope efficiency obtained from the pulse tests is smaller for rods having higher scattering losses, in spite of the fact that these slope efficiencies were obtained using a high output coupling [for  $R = 0.35$  and  $\alpha_s L = 0.2$ , the output coupling from Eq. (8) is 0.73]. The coupling is very low during the continuous laser tests (for 97% reflectivity and  $\alpha_s L = 0.2$ , the output coupling is only 0.07) and thus the internal scattering of the stimulated emission has a significant effect upon the slope efficiency.

The pulse laser tests indicated that FAP:Nd has four to five times greater gain than YAG:Nd when excited by the same energy into a xenon-filled flashlamp. This factor is probably not greatly different for tungsten lamp excitation. Therefore, the higher gain of FAP:Nd is just sufficient to compensate for its higher losses so that the FAP and YAG rods have similar cw threshold powers. However, the higher scattering losses of the FAP:Nd rods reduce their output efficiencies to a greater extent than those of YAG:Nd.

## Conclusions

The analysis of the spectroscopic and laser test results indicate that neodymium-doped calcium fluorophosphate (FAP:Nd) has emission and absorption properties that make it useful as a crystalline laser material. It has a higher gain at the laser transition than YAG:Nd for equal energy into the pumping lamp and a higher efficiency than YAG:Nd under pulse excitation. The reason for the intrinsically higher gain and efficiency of FAP:Nd over YAG:Nd may be traced back to the fluorescence and absorption spectra. The low symmetry of the Nd site in FAP causes many over-

lapping lines to appear in the absorption spectrum, and that results in a relatively high average absorption of broad band pump radiation. In addition, a relatively large fraction of the fluorescence of FAP:Nd appears in a single line in one polarization. This fact means that the intrinsic gain per unit absorbed pump power is high. The decay time of FAP:Nd is almost equal to that of YAG:Nd since the total oscillator strengths of the transitions from the  ${}^4F_{3/2}$  state to all lower states and the quantum efficiencies are about equal in the two materials.

The crystal quality of FAP:Nd has not yet been perfected to that of the best YAG:Nd laser crystals. Owing to the losses, the efficiencies of continuous FAP:Nd lasers are not as high as the efficiency of a comparable size YAG:Nd laser. It is not yet clear whether the lower thermal conductivity of fluorapatite will prove an ultimate limitation on continuous laser output power, or whether this may be overcome by using long laser rods so that the heat absorbed per unit volume may be kept small.

The authors acknowledge the many technical discussions with T. Henningsen, R. D. Haun, Jr., J. Murphy, and I. Liberman. The spectroscopic studies were greatly aided by R. Pervuznik and R. Muth. Laser performance measurements were ably carried out by T. Henningsen and R. Madia. W. Kramer and E. Metz assisted in the development of crystal growth techniques.

This work was supported in part by a contract from the National Aeronautics and Space Administration.

## References

1. W. V. Smith and P. P. Sorokin, *The Laser* (McGraw-Hill Book Co., Inc., New York, 1966), p. 125.
2. A. A. Kaminskii and V. V. Osiko, *Inorg. Mater.* **1**, 1853 (1965) [*Izv. Akad. Nauk SSSR, Neorg. Mat.* **1**, 2049 (1965)].
3. J. E. Geusic, H. W. Marcos, and L. G. Van Uitert, *Appl. Phys. Letters* **7**, 127 (1965).
4. L. F. Johnson and K. Nassau, *Proc. Inst. Radio Eng.* **49**, 1705 (1961); L. F. Johnson, G. D. Boyd, K. Nassau, and R. R. Soden, *Proc. Inst. Radio Eng.* **50**, 213 (1962); *Phys. Rev.* **126**, 1406 (1962); L. F. Johnson, *J. Appl. Phys.* **34**, 897 (1963).
5. J. R. O'Connor, *Appl. Phys. Letters* **9**, 407 (1966).
6. K. B. Steinbruegge, R. C. Ohlmann, and R. Mazelsky, *Bull. Amer. Phys. Soc.* **12**, 90 (1967).
7. P. D. Johnson, *J. Electrochem. Soc.* **108**, 159 (1961).
8. R. Mazelsky, R. C. Ohlmann, and K. B. Steinbruegge, *J. Electrochem. Soc.* **115**, 68 (1968).
9. St. Naray-Szabo, *Z. Kristallogr.* **75**, 387 (1930); S. S. Hendricks, M. E. Jefferson, and U. M. Mosley, *Z. Kristallogr.* **81**, 352 (1931); R. A. Young and J. C. Elliot, *Arch. Oral Biol.* **11**, 699 (1966).
10. R. A. Buchanan, K. A. Wickersheim, J. J. Pearson, and G. F. Herrmann, *Phys. Rev.* **159**, 245 (1967).
11. G. F. Koster, J. O. Dimmock, R. G. Wheeler, and H. Statz, *Properties of the Thirty-Two Point Groups* (MIT Press, Cambridge, Massachusetts, 1963), pp. 33, 51.
12. R. G. Wagner, Westinghouse Research Laboratories, Pittsburgh, private communication.
13. R. Ladenberg, *Z. Physik* **4**, 451 (1921); W. B. Fowler and D. L. Dexter, *Phys. Rev.* **128**, 2151 (1962); D. F. Nelson and M. D. Sturge, *Phys. Rev.* **137**, A1117 (1965).

14. R. J. Pressley and P. V. Goedertier, Tech. Rept. #AFAL-TR-67-100, May 1967, available from the Defense Documentation Center, Washington, D. C., as report #AD814949.
15. W. W. Piper, L. C. Kravitz, and R. K. Swank, Phys. Rev. **138**, A1802, 1965; R. K. Swank, Phys. Rev. **135**, A266 (1964); P. D. Johnson, J. Appl. Phys. **32**, 127 (1961).
16. D. Findlay and R. A. Clay, Phys. Lett. **20**, 277 (1966); D. W. Goodwin, Phys. Lett. **24A**, 283 (1967).
17. P. A. Miles and I. Goldstein, IEEE Trans. **ED-10**, 314 (1963).
18. C. Church and I. Liberman, Appl. Opt. **6**, 1966 (1967).

Unusual or Neglected Optical Phenomena in the Landscape . . . . .	M. G. J. Minnaert	297
Optical Back Scattering from Single Water Droplets . . . . .	T. S. Fahlen and H. C. Bryant	304
Laser-Excited Rotation-Vibration Raman Scattering in Ultrasmall Gas Samples . . . . .	J. J. Barrett and N. I. Adams, III	311
Optical Modes of Vibration in an Ionic Crystal Sphere. . . . .	Ronald Fuchs and K. L. Kliever	316
Spectra of Ions in the Fluorine I Isoelectronic Sequence from Sc XIII to Cu XXI . . . . .	Leonard Cohen, U. Feldman, and S. O. Kastner	331
Absorption of Infrared Radiation by CO <sub>2</sub> and H <sub>2</sub> O. II. Absorption by CO <sub>2</sub> between 8000 and 10000 cm <sup>-1</sup> (1-1.25 Microns) . . . . .	Darrell E. Burch, David A. Gryvnak, and Richard R. Patty	335
Theoretical Prediction of Image Quality . . . . .	P. G. Roetling, E. A. Trabka, and R. E. Kinzly	342
Optimization of Information-Processing Optical Systems by Transcorrelation-Function Maximization . . . . .	R. S. Macmillan and G. O. Young	346
Effect of the Photographic Gamma on the Luminance of Hologram Reconstruction . . . . .	James C. Wyant and M. Parker Givens	357
Parallel Wood's Anomalies of Optical Gratings. . . . .	Shiro Fujiwara and Yasuo Iguchi	361
Thickness Calculations for a Transparent Film from Ellipsometric Measurements . . . . .	Mario Ghezzi	368
Optical Properties of As <sub>2</sub> Se <sub>3</sub> , (As <sub>x</sub> Sb <sub>1-x</sub> ) <sub>2</sub> Se <sub>3</sub> , and Sb <sub>2</sub> S <sub>3</sub> . . . . .	A. Efstathiou and E. R. Levin	373
Refractive Index and Low-Frequency Dielectric Constant of 6H SiC . . . . .	W. J. Choyke and Lyle Patrick	377
Electric Fields Produced by the Propagation of Plane Coherent Electromagnetic Radiation in a Stratified Medium . . . . .	Wilford N. Hansen	380
Typical Spectral Distribution and Color for Tropical Daylight . . . . .	V. D. P. Sastri and S. R. Das	391
Perspective and the Rotating Trapezoid . . . . .	Myron L. Braunstein and John W. Payne	399
Critical Duration, the Differential Luminance Threshold, Critical Flicker Frequency, and Visual Adaptation: A Theoretical Treatment . . . . .	Leonard Matin	404
Determination of Small Birefringence in the Bovine Lens Capsule by Optical Rotatory Dispersion . . . . .	Noriaki Takeguchi and Masayuki Nakagaki	415
Optimizing the Use of the Criterion Response for the Pupil Light Reflex . . . . .	John G. Webster, Gerald H. Cohen, and Robert M. Boynton	419
Recovery Time of Cats Following High-Luminance Stimulation . . . . .	David I. Randolph	424
<b>Letters to the Editor:</b>		
Correction Factors for Polarized Spectroscopy . . . . .	Isaac Freund	427
Duc de Chaulnes' Method for Refractive-Index Determination . . . . .	Arthur Miller	428
Helium 3 <sup>2</sup> D Fine Structure . . . . .	R. D. Kaul	429
Opponent-Response Functions Related to Measured Cone Photopigments . . . . .	Dorothea Jameson and Leo M. Hurvich	429
Atomic-Absorption Cross Sections of Na, 500 to 600 Å . . . . .	Robert D. Hudson and Virginia L. Carter	430
Propagation of the Coherence Function through Random Media . . . . .	M. Beran	431
Simplified Method to Make Hologram Filters for Target Recognition . . . . .	Dominic J. Raso	432
Comparison of the Radiance of Far-Infrared Sources . . . . .	Donald R. Smith, Robert L. Morgan, and Ernest V. Loewenstein	433
Field of View and Resolution of a Polarization Fourier Spectrometer . . . . .	James E. Stewart	434
Effects of Film-Grain Noise in Holography . . . . .	Adam Kozma	436
<b>Book Reviews:</b>		
Generation of Optical Surfaces. Edited by K. G. Kumanin . . . . .	Reviewed by J. M. McLeod	438
Aerial Discovery Manual. By Carl H. Strandberg . . . . .	Reviewed by Eugene A. Trabka	438
Optical Properties of III-V Compounds. By R. K. Willardson and Albert C. Beer . . . . .	Reviewed by Benjamin B. Snavely	439
Lumière et Vie Animale. By Yves Le Grand . . . . .	Reviewed by Mathew Alpern	439
Selected Readings in Physics: Atomic Spectra. By W. R. Hindmarsh . . . . .	Reviewed by William C. Martin	439
Announcements . . . . .		440
Contents. . . . .		440
OSA Technical Groups . . . . .		441
Personalia . . . . .		442
Technical Calendar . . . . .		444
Local Section Calendar . . . . .		444
From the Executive Office . . . . .		445
Editor's Page . . . . .		446